Evolution of magnetic and transport properties in the Cu-doped pyrochlore iridate $Eu_2(Ir_{1-x}Cu_x)_2O_7$

Sampad Mondal,[1,2,3,*] M. Modak,[2] B. Maji,[4] Swapan K. Mandal,[1] B. Ghosh,[5] Surajit Saha,[5] M. Sardar,[6] and S. Banerjee[2,†]

[1]*Department of Physics, Visva-Bharati, Santiniketan 731235, India*
[2]*Saha Institute of Nuclear Physics, 1/AF Bidhannagar, Kolkata 700064, India*
[3]*Ramsaday College, Amta, Howrah 711401, India*
[4]*Acharya Jagadish Chandra Bose College, 1/1B, A. J. C. Bose Road, Kolkata 700020, India*
[5]*Department of Physics, Indian Institute of Science Education and Research, Bhopal 462066, India*
[6]*Material Science Division, Indira Gandhi Centre for Atomic Research, Kalpakkam 603102, India*

(Received 19 July 2021; accepted 18 March 2022; published 7 April 2022)

We have investigated the effect of Cu substitution in $Eu_2(Ir_{1-x}Cu_x)_2O_7$ with the help of magnetic and transport property measurements. XPS measurement reveals that each Cu^{2+} converts Ir^{4+} to double the amount of Ir^{5+} ions. The metal-insulator transition temperature (T_{MI}) is obtained around 120 K. In the insulating phase, at lower temperature below 50 K, the temperature-dependent resistivity follows a power-law dependence and the magnitude of the exponent increases with Cu concentrations. The temperature-dependent thermopower is observed to follow the electrical resistivity down to 50 K, except for a sudden drop in thermopower at temperature below 50 K. We find negligible Hall voltage in the metallic regime of the samples but a sudden Hall voltage is developed below 50 K. We observe bifurcation in zero-field-cooled and field-cooled (ZFC-FC) magnetization below irreversibility temperature, exchange bias, and negative magnetoresistance at 3 K and the magnitude of all these properties increases with Cu concentrations. In the insulating region (below 6 K) there exists a linear specific heat and its coefficient decreases with Cu doping, which indicates the reduction of spinon contribution with Cu doping.

DOI: 10.1103/PhysRevB.105.155113

I. INTRODUCTION

Unlike 3*d* and 4*d* transition metal oxides, there exists a relativistic spin-orbit interaction in Hamiltonian in 5*d* transition metal oxide compounds. The competition of spin-orbit interaction and electronic correlation energy U gives rise to a rich variety of novel quantum-correlated phases such as quantum spin liquid, Weyl semimetal, and axion insulator [1–4]. In 5*d* transition metal oxide compound, for example, layered iridium oxide Sr_2IrO_4 system [5], Ir is in charge state Ir^{4+} ($5d^5$). The crystal-field effect due to the environment of IrO_6 octahedra splits the 5*d* orbital into t_{2g} and e_g levels. In the presence of spin-orbit coupling (SOC), the lower-energy level t_{2g} further splits into two bands with fully filled spin $J_{\text{eff}} = \frac{3}{2}$ quadruplet and partially filled spin $J_{\text{eff}} = \frac{1}{2}$ doublet. The electron correlation further splits the $J_{\text{eff}} = \frac{1}{2}$ band and opens a Mott gap at the Fermi level (E_F). Thus, the interplay of SOC and U provides a stage for the study of a wide range of quantum-correlated phenomena.

Among the 5*d* transition metal oxide compounds, pyrochlores are the most promising system to tune SOC and U because of their interpenetrating corner-sharing tetrahedral structure. It tends to form a narrow flat band at the Fermi level and the bandwidth is comparable to energy scale of SOC and U. Particularly, $R_2Ir_2O_7$ (R = rare earth) shows an intriguing behavior in their exotic transport and magnetic properties depending on the ionic radius of the rare-earth atom [6–8]. In the pyrochlore family, R = Nd-Sm shows metal-insulator transition with an all-in–all-out antiferromagnetic spin ordering at insulating state. Recently, it has been theoretically predicted that this compound shows novel correlated quantum phenomena including topological insulator, Weyl semimetal, and axion insulator [4,9–11]. In a magnetically ordered system, where time-reversal symmetry is broken but inversion symmetry is preserved, a quadratic band-touching point leads to a linear dispersing Dirac-fermion-like spectrum, along with definite spin chirality, i.e., $\bar{k} \cdot \bar{\sigma} = \pm 1$, where $\bar{k}$ and $\bar{\sigma}$ are the unit vectors along the momentum and spin of the electron, respectively. This promotes the formation of a Weyl-semimetal-like phase in this compound. In the strong correlation limit, the preexisting narrow bands due to spin-orbit coupling may open up a gap. For an increase in Coulomb correlation energy, a pair of Weyl points with opposite chirality moves towards the Brillouin zone boundary and annihilates pairwise to open up a gap forming a spin-orbit-assisted Mott insulator [9]. If there exists frustration in the magnetic exchange interaction (like in the pyrochlore compounds), then one may get either metallic or insulating spin-liquid phase [12].

To study such exotic ground-state properties in details, the pyrochlore iridate $Eu_2Ir_2O_7$ has drawn special interest.

*sampad100@gmail.com
†sangam.banerjee@saha.ac.in

In such a compound, one can not only observe thermally induced metal-insulator transition, but also can avoid f-d exchange interaction [13] for nonmagnetic Eu^{3+} ions. This allows us to study the Ir sublattice without the phenomena emerging from interaction with rare-earth ion and Ir^{4+} ion. The Weyl semimetal signature for $Eu_2Ir_2O_7$ was confirmed by Tafti *et al.* [14] comparing with the calculated resistivity data [15] for the Weyl semimetal. Recently, Telang *et al.* [16] also reported the Weyl semimetal nature in the polycrystalline $Eu_2Ir_2O_7$ compound by doping Bi at Eu site. All the above features make this system ideal for studying the interplay between SOC and U associated to the system. Substituting Ir by a 3d or 4d element, one can tune the SOC and electronic correlation energy which can modify the physical property of the system [17,18]. Previously, Banerjee *et al.* [19] showed that nonmagnetic divalent element doping at Eu site creates a Ir^{4+}/Ir^{5+} charge disproportion, which led the system toward a non-Fermi-liquid state.

In this work, we have studied the effect of Cu doping at Ir site in $Eu_2(Ir_{1-x}Cu_x)_2O_7$ compound. To be mentioned, Ir^{4+} has higher SOC and lower U compared to Cu^{2+}. Substitution of Cu^{2+} in the Ir^{4+} site not only changes the SOC and U in the system, but also changes the state of Ir^{4+} to Ir^{5+}, and acts as site dilution for creating a nonmagnetic Ir^{5+} charge state. We observe insignificant change in T_{MI} with Cu doping and $T_{MI} = T_{irr}$ (irreversibility temperature) is maintained for all the compounds. Upon doping of Cu at Ir site, each Cu creates double the amount of Ir^{5+}, thus each corner-shared tetrahedron deviates from its all-in–all-out (AIAO) spin structure and picks up a moment, which leads to a small ferrocontribution in those droplet regions (note: this supermoment droplet we shall refer to as ferrocontribution in this paper) dispersed within a background of antiferromagnetic all-in–all-out (AFM AIAO) spin structure. It is believed that quantum fluctuations could stabilize a so-called resonating valence bond (RVB) state. The resulting RVB state is a liquidlike state of spins [20]. The prerequisite condition for spin-liquid formation is AFM spin structure and, hence, with an increase in Cu doping the spinon contribution (fractional excitation for the spin liquid) region is found to be decreased. In this paper, we shall address this in more details, and also its manifestations in physical properties such as in magnetic, electrical, and thermal behavior will be discussed.

II. EXPERIMENTAL DETAILS

All the polycrystalline samples were prepared by a solid-state reaction method. High-purity ingredient powder Eu_2O_3, IrO_2 and CuO with phase purity 99.9% (Alfa Aesar) were mixed in stoichiometric ratio and grounded well. After pressing the mixture powder in pellet form, the sample was heated at 1273 K for 3 days with several intermediate grindings. All the samples were characterized by powder x-ray diffraction (XRD) and x-ray photoelectron spectroscopy (XPS). The room-temperature XRD measurement was carrried out by x-ray diffractometer with Cu K_α radiation. Structural parameters were determined using the standard Rietveld technique with FULLPROF software package. XPS measurements at room temperature were carried out by using an Omicron Multiprobe Electron Microscopy System equipped with a monochromatic

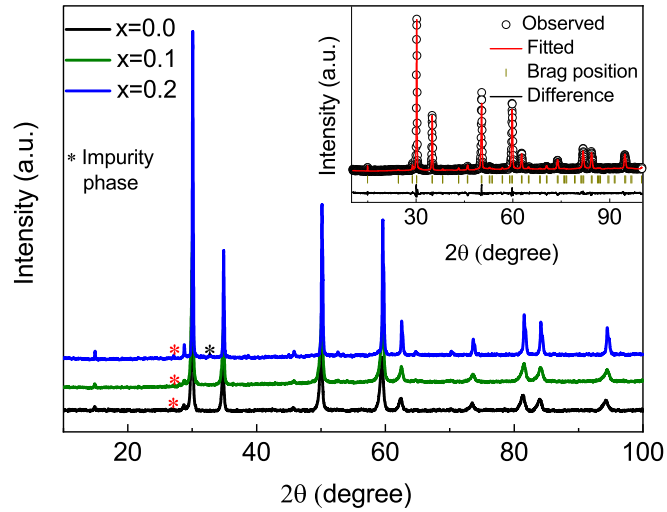

FIG. 1. Room-temperature x-ray diffraction pattern of $Eu_2(Ir_{1-x}Cu_x)_2O_7$, where $x = 0$, 0.1, 0.2 and red and black stars indicate the impurity phases due to nonreacting IrO_2 and Eu_2O_3, respectively. Inset shows Rietveld refinement for the $x = 0.1$ compound, where scattered data are observed and the solid line is fit to the data.

Al K_α x-ray source ($h\nu = 1486.7$ eV). All the XPS spectra have been analyzed by using PEAKFIT software, where the Shirley method was used for background subtraction. Magnetic measurements were performed using superconducting quantum interference device magnetometer (SQUID-VSM) of Quantum Design in the temperature range 3–300 K. Electrical, magnetic, and thermal transport measurements were carried out by the four-probe method with a temperature range 2–300 K using Physical Properties Measurement System (PPMS). To determine the Hall coefficient, we have measured the Hall resistance with applied fields of opposite polarities, and subtracted one from the other.

III. EXPERIMENTAL RESULTS

Room-temperature XRD pattern of $Eu_2(Ir_{1-x}Cu_x)_2O_7$ with $x = 0, 0.1, 0.2$ are shown in Fig. 1. XRD patterns of doped and parent samples appear similar. Rietveld refinement for all the compounds has been performed considering cubic structure with Fd-3m space group, one of which ($x = 0.1$) has been shown in the inset of Fig. 1. All the samples are nearly in pure phase with some minor impurity phases (nonreacting oxide), indicated by red and black stars. The obtained lattice parameters for $x = 0$, 0.1, and 0.2 compounds are 10.3048 ± 0.0004, 10.2778 ± 0.0001, and 10.2777 ± 0.0001 Å, respectively. The lattice parameter decreases upon Cu doping.

It is important to know the charge state of transition metal in this compound as it dominates the electronic and magnetic properties. Therefore, we have carried out x-ray photoelectron spectroscopy (XPS) measurement for all the samples. Figures 2(a)–2(c) depict the Ir 4f core-level spectra for $x = 0$, 0.1, and 0.2, respectively. Spin-orbit coupling (SOC) splits the Ir 4f core level into $4f_{7/2}$ and $4f_{5/2}$ electronic states around binding energy 62 and 65 eV, respectively (as shown by dashed blue line) for Ir^{4+}. The spectra for all the samples

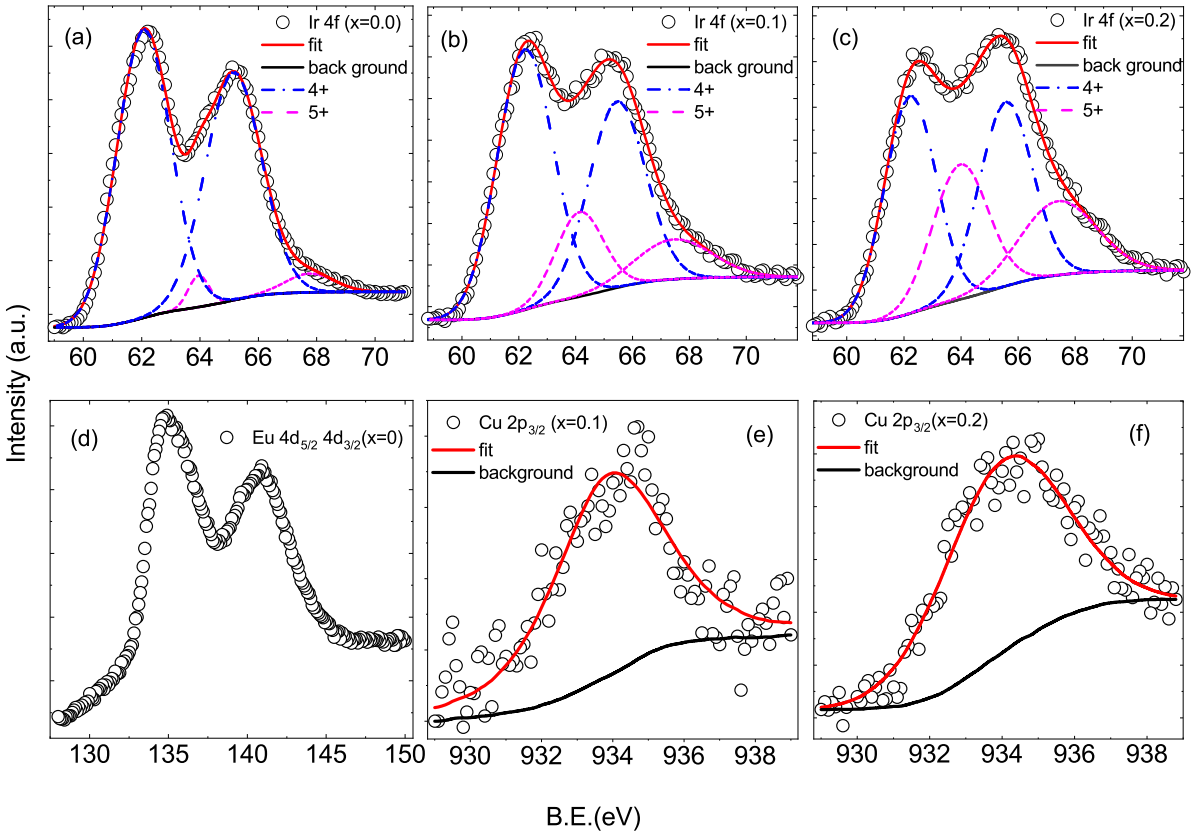

FIG. 2. (a)–(c) Ir $4f$ core-level x-ray photoelectrons spectra for $x = 0$, 0.1, 0.2 compounds, respectively. (d) Eu $4d$ spectra for $x = 0$ and (e), (f) Cu $2p_{3/2}$ core-level spectra for $x = 0.1$, 0.2. Open black circles are experimental data and solid red lines are fitted data.

can be fitted taking the peaks due to Ir^{4+} with some weak additional peaks occurring at the higher binding energy 64 and 67.7 eV (as shown by pink dotted line). These additional peaks correspond to $4f_{7/2}$ and $4f_{5/2}$ states of Ir^{5+} ion. We observe a small increase in intensity of the Ir^{5+} peak compared to Ir^{4+} for the $x = 0$ compound. The calculation of area under the curve of the XPS spectrum reveals that for $x = 0$ compound, the amounts of Ir^{4+} and Ir^{5+} are 95.9% and 4.1%, respectively. In the parent sample, the majority of Ir is in the Ir^{4+} state. The small amount of Ir^{5+} in the $Eu_2Ir_2O_7$ could be due to unavoidable nonstoichiometry of the sample [21,22]. We observe a significant increment in the intensity of Ir^{5+} peaks compared to Ir^{4+} in doped compounds and the amount of Ir^{4+} and Ir^{5+} in $x = 0.1$, 0.2 compounds are found as 77.7% and 22.3% and 60.1% and 39.9%, respectively. Now, if we consider Ir^{5+} contribution due to the nonstoichiometry of the sample, then 10% and 20% substitution of Cu produces roughly 18.2% and 35.8% Ir^{5+}, respectively. Hence, each Cu ion converts two Ir^{4+} to Ir^{5+} ions. Figure 2(d) shows that Eu $4d_{5/2}$ and $4d_{3/2}$ core-level spectra with peak position at 134.7 and 140.9 eV, respectively. To further investigate the charge state of Cu in this compound, we have taken Cu $2p_{3/2}$ core-level spectra for $x = 0.1$ and 0.2, respectively, shown in Figs. 2(e) and 2(f). Red lines are fit to the observed data with $2p_{3/2}$ spectra centered around the binding energy 934 eV, which confirms that Cu stays at Cu^{2+} oxidization state.

Resistivity measurements, carried out as a function of temperature, are presented in Fig. 3(a). All the samples show metal-to-insulator transition (MIT), which is clearly observed from the inset in Fig. 3(a) where $d\rho/dT$ changes from positive to negative at lower temperature. Metal-insulator transition temperatures (T_{MI}) for the compounds $x = 0$, 0.1, and 0.2 are 120, 113, and 115 K, respectively. Cu doping shifts the T_{MI} to lower temperature compared to the parent compound and the resistivity is higher than the parent compound in the entire temperature range.

For further analysis of the resistivity data at low temperature, we have tried to fit the data below T_{MI} for all the samples with power law

$$\rho = \rho_0 T^{-\alpha}, \tag{1}$$

where α is the exponent, as shown in Fig. 3(b). The fitted parameter and temperature region are shown in Table I. All the data fit well over a limited temperature range (around one order of magnitude, i.e., 3–50 K) and the α value is found to increase with Cu concentration. Power-law behavior signifies that it is not an activated process and could be a continuous transition to a fluctuating disorder state.

TABLE I. Fitting parameters α obtained from power-law fitting for the samples $Eu_2(Ir_{1-x}Cu_x)_2O_7$.

Sample	Temperature range (K)	α
$x = 0$	4.5–23	0.531 ± 0.006
$x = 0.1$	3–51	1.446 ± 0.007
$x = 0.2$	5–49	1.61 ± 0.01

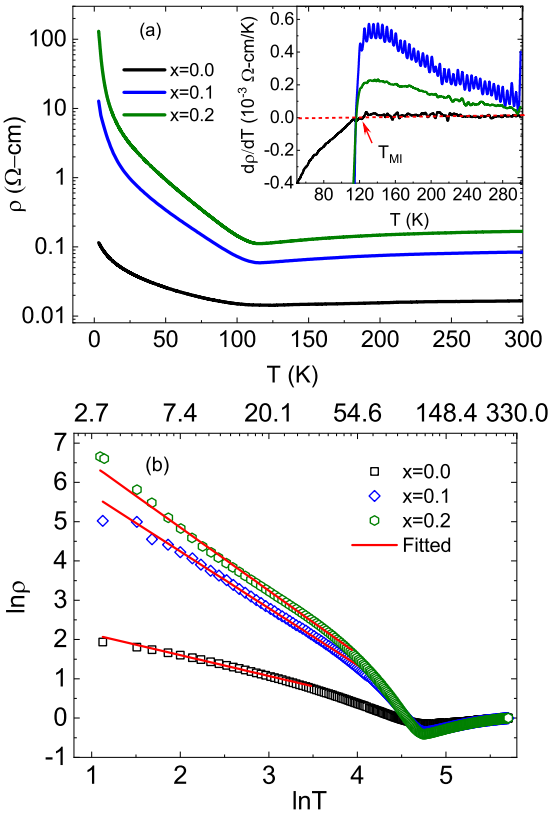

FIG. 3. (a) Temperature-dependent resistivity measured in the temperature range 2.1–300 K for $Eu_2(Ir_{1-x}Cu_x)_2O_7$. Inset: temperature derivative of the resistivity as a function of temperature. (b) ln-ln plot of the $\rho(T)$ data for all the compounds and solid red lines are power-law fitting of the observed data.

In a three-dimensional disordered system, Mott variable range hopping can be expected. Therefore, we have also tried to fit the resistivity data with three-dimensional Mott variable range hopping model (VRH) [23]

$$\rho = \rho_0 \ \exp[(T_0/T)^{1/4}], \tag{2}$$

where $T_0 = \frac{21.2}{N(E_F)\xi^3}$, $N(E_F)$ and ξ are density of states at the Fermi level and localization length. All the samples can be fitted with a limited temperature region 3–10 K. So, we do not claim the system to be a strongly localized since the fitting temperature range is narrow (less than one order of magnitude).

We have measured the temperature-dependent Seebeck coefficient (S) as shown in Fig. 4. The overall behavior of $S(T)$ for $x = 0$ is in agreement with the previous paper [7,16]. The nature of the temperature-dependent S for doped samples is similar to the parent compound. For all the samples, S is found to decrease monotonically from room temperature down to T_{MI}, which is the expected behavior of a metal. On further reduction of temperature, S starts rising and at lower temperature below 50 to 30 K, a sudden drop is observed giving rise to a peak. This characteristic peak is possibly due to phonon-drag contribution as discussed in previous papers [7,16,24,25]. However, in this temperature range, the resistivity increases obeying power-law behavior with reduction in temperature. This plausibly suggests a spin-liquid-like

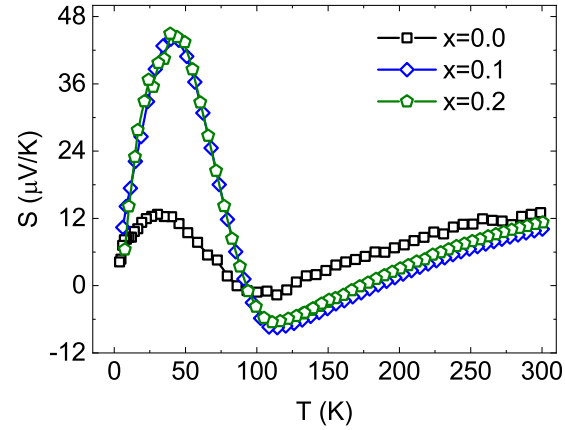

FIG. 4. Temperature variation of thermoelectric power (S) for $Eu_2(Ir_{1-x}Cu_x)_2O_7$, where $x = 0, 0.1, 0.2$.

signature that will be explored later from the low-temperature heat-capacity measurement.

We have also measured the Hall coefficient (proportional to the measured Hall voltage) as a function of temperature, with applied field 50 kOe for the parent and doped compounds, as shown in Fig. 5. Hall voltage is negligible above T_{MI} but below 50 to 30 K, a steep negative Hall voltage is found to be developed. We have also observed a drop in thermopower in the very similar temperature range (see Fig. 4). The sudden development of the negative Hall voltage is possibly due to the onset of electron spin fluctuation affected by the applied perpendicular magnetic field. Although all the compounds show negative Hall coefficient (R_H) at low temperature, its magnitude for the doped sample is observed to be higher than the parent sample. It indicates that the majority charge carriers

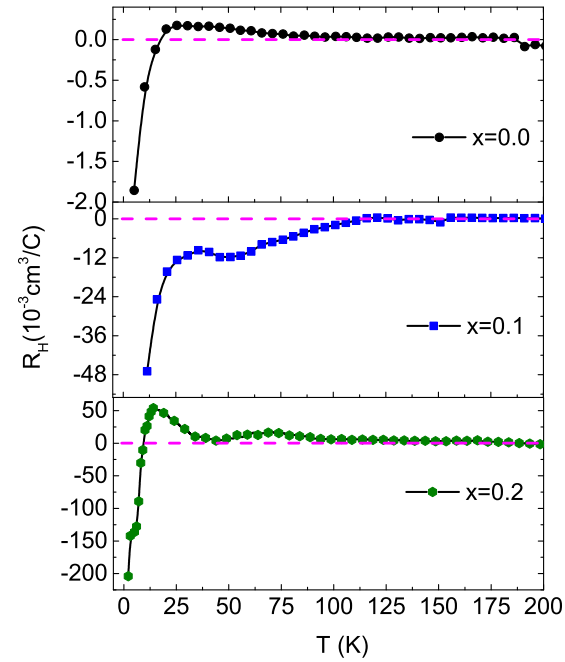

FIG. 5. Temperature-dependent Hall coefficient with applied field 50 kOe for $Eu_2(Ir_{1-x}Cu_x)_2O_7$, where $x = 0$, 0.1, and 0.2.

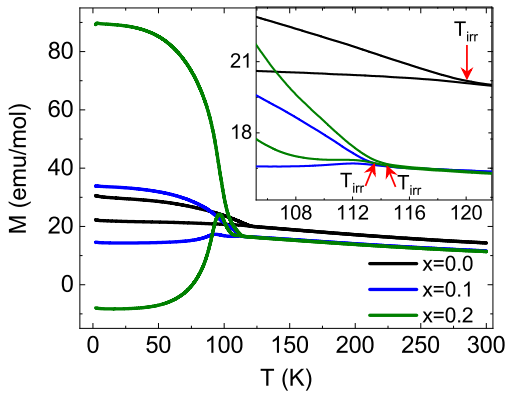

FIG. 6. Temperature-dependent magnetization measured at 1 kOe in ZFC FC protocol for $Eu_2(Ir_{1-x}Cu_x)_2O_7$, where $x = 0$, 0.1, 0.2. Inset: enlarged view of the irreversibility temperature.

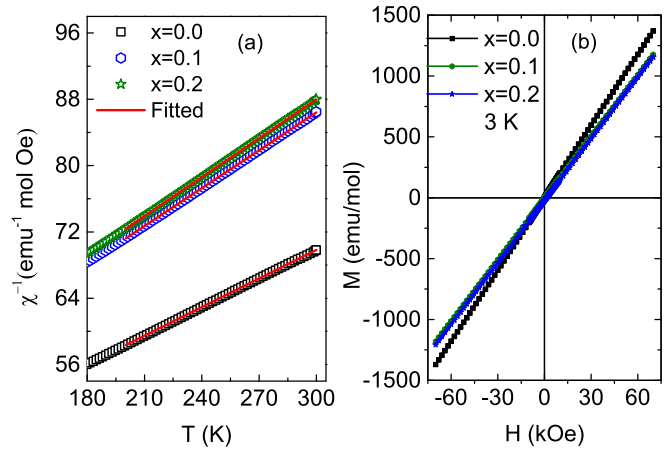

FIG. 7. (a) Temperature-dependent inverse susceptibility with Curie-Weiss fit. (b) Isothermal magnetization at 3 K for $Eu_2(Ir_{1-x}Cu_x)_2O_7$, where $x = 0$, 0.1, 0.2.

at low temperature for all the compounds are electronlike, whereas the carrier concentration decreases with Cu doping.

Figure 6 represents temperature-dependent magnetization (M) for all the samples under zero-field-cooled (ZFC) and field-cooled (FC) protocols with applied field 1 kOe. Parent sample shows a magnetic irreversibility around $T_{irr} = 120$ K, below which there is a bifurcation between the ZFC and FC curves. Such type of magnetic behavior was reported in the literature [21]. From resonant x-ray diffraction (RXD) and muon spin rotation and relaxation (μSR) studies, it was revealed that in this compound below T_{irr}, Ir moments order in an antiferromagnetic all-in–all-out spin arrangement [26,27]. We observe that T_{irr} for $x = 0$, 0.1, and 0.2 compounds are near about 120, 113, and 115 K, respectively (see inset in Fig. 6). Therefore, all the compounds undergo metal-insulator transition almost at their respective irreversibility temperature. There exhibits a prominent cusp in the ZFC magnetization around T_{irr} for all the compounds. We observe that the difference between M_{ZFC} and M_{FC} is systematically increased with Cu doping. The ZFC magnetization below T_{irr} gradually shifts to lower value with doping. (Note: The negative magnetization observed in the ZFC for $x = 0.2$ is due to the small negative field trap in the instrument while cooling in zero-field condition and is attributed to an instrumental artifact.) Since each Cu ion creates two Ir^{5+} nonmagnetic ions, as a result, the ZFC magnetization of the system decreases with doping. On the other hand, the FC magnetization is found to increase with Cu doping. This further indicates an increase in field-induced magnetization with an increase in doping concentrations. Bifurcation is observed due to formation of field-induced ferrocorrelation within the droplets containing Cu with the applied magnetic field (i.e., in those regions where AIAO deviates due to Cu^{2+} doping). These droplets are dispersed in an AIAO AFM background matrix and the flat plateau observed at very low temperature indicates that these ferrodroplets are randomly arrested and frozen in the AIAO AFM background matrix. With an increase in temperature, these supermoments tend to unblock, giving rise to the observed bifurcation below T_{irr}.

Figure 7(a) shows temperature-dependent inverse susceptibility for $x = 0$, 0.1, 0.2, fitted in the temperature region 200–300 K with the Curie-Weiss law $\chi = \frac{C}{T-\theta p}$, θp is the Curie-Weiss temperature, Curie constant $C = \frac{N_A \mu_{\text{eff}}^2}{3K_B}$, and μ_{eff} is the effective paramagnetic moment. The fitted parameters μ_{eff} and θ_p and frustration parameter ($f = |\theta_p|/T_{irr}$ indicates the level of frustration in the system) are listed in Table II. All the samples show negative θ_p, which indicates antiferromagnetic interaction, whose strength decreases with Cu doping. We also observe that frustration parameter f decreases with Cu doping, which signifies the decrease in frustration with Cu concentration. From XPS measurement, we observed that x amount of Cu^{2+} creates $2x$ amount of Ir^{5+}, hence, the effective moment can be expressed as

$$\mu_{\text{eff}} = \sqrt{(1-3x)\left(\text{Ir}^{4+}_{\mu_{\text{eff}}}\right)^2 + 2x\left(\text{Ir}^{5+}_{\mu_{\text{eff}}}\right)^2 + x\left(\text{Cu}^{2+}_{\mu_{\text{eff}}}\right)^2}. \quad (3)$$

As Ir^{5+} is nonmagnetic, the effective moment decreases with Cu concentration.

The isothermal magnetization curve (M-H) for all the samples measured at 3 K up to field 70 kOe is shown in Fig. 7(b). All the compounds show linear behavior without any hysteresis. The magnetic moment at the highest applied magnetic field (70 kOe) decreases with Cu doping. The reduction of moment with Cu doping is due to the creation of nonmagnetic Ir^{5+} ions.

The magnetic field cooled M-H were measured at 3 K after the samples were cooled down from room temperature in presence of a magnetic field at 1 and −1 kOe. From Fig. 8(a), we observe a shift of the M-H curve along the magnetization axis for $x = 0$ and 0.2 compounds. The direction of the shift depends on the polarity of the field. The magnitude of the shift increases with Cu doping though there is no hysteresis loop

TABLE II. μ_{eff}, θ_p, and f for $Eu_2(Ir_{1-x}Cu_x)_2O_7$ system.

Sample	μ_{eff} (μ_B/f.u.)	θ_p (K)	f
$x = 0$	8.32	-306.2 ± 0.2	2.551 ± 0.002
$x = 0.1$	7.24	-267.4 ± 0.1	2.3663 ± 0.0009
$x = 0.2$	7.14	-262.8 ± 0.1	2.2852 ± 0.0009

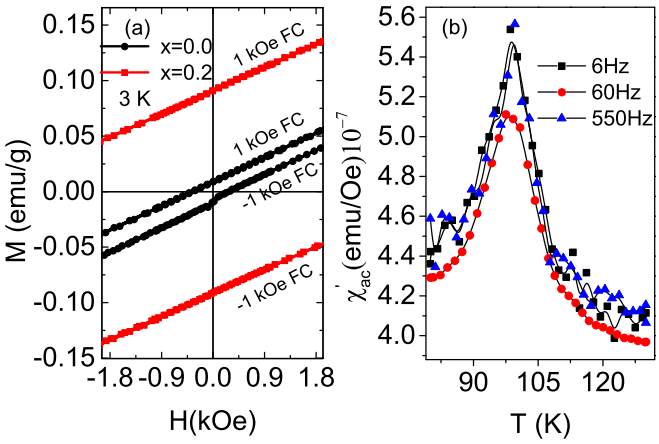

FIG. 8. (a) Isothermal magnetization at 3 K after the sample was cooled in presence of magnetic field at 1 and −1 kOe for $Eu_2(Ir_{1-x}Cu_x)_2O_7$, where $x = 0$, 0.2. (b) Temperature-dependent ac susceptibility for $x = 0.2$ compound with different frequencies.

for both the compounds. Such type of cooling-field-induced shift of the *M-H* curve has been previously observed in the pyrochlore iridates [28]. Since each corner-shared tetrahedra deviates from its all-in–all-out spin structure and it picks up a moment in both the samples ($x = 0$ and 0.2) due to creation of nonmagnetic Ir^{5+} state, leading to a small ferrocontribution. This ferrocontribution interacts with background AIAO AFM spin matrix, giving an additional exchange field due to pinning with the ferrospin and produces exchange-bias-like behavior. The size and amount of the ferroisland or ferrodroplets increases with an increase in Cu concentration. This leads to larger amount of ferroisland pinning to the AIAO AFM background and, hence, increases the shift (exchange bias) of the *M-H* curve with increase in Cu doping.

The ac magnetization measurement is an efficient tool to detect the existence of nonequilibrium phase in the compound. We have carried out temperature-dependent ac susceptibility measurement for an $x = 0.2$ compound at different frequencies as shown in Fig. 8(b). A peak at $T = 95$ K was observed and does not shift with frequency. This confirms that there is no glassylike dynamics below the T_{irr} in the doped compound and further reflects the AFM phase transition.

Magnetoresistance (MR) is defined by $(\rho_H - \rho_0)/\rho_0$, where ρ_H and ρ_0 are the resistivity with field and without field. Figure 9(a) shows temperature-dependent MR for the $x = 0.1$ compound. We observe that below T_{MI}, MR is negative. MR as a function of magnetic field measured at 3 K [Fig. 9(b)] shows a negative value for all the samples. The magnitude of the negative MR increases with Cu doping due to an increase of field-induced ferrocontribution regions where the spin-flip scattering is lower than that of the AIAO AFM structure.

Figures 10(a)–10(c) show specific-heat data as a function of temperature for all the samples in the temperature range 20–200 K. The vertical dotted line in C/T vs T data for all the samples marks the expected anomaly. We do not observe any anomaly for $x = 0$ but we clearly observe for $x = 0.1$ and 0.2 at 110 and 112 K, respectively. This anomaly temperature is close to the magnetic irreversibility temperature (T_{irr}). To determine the change of electronic contribution γ, we have

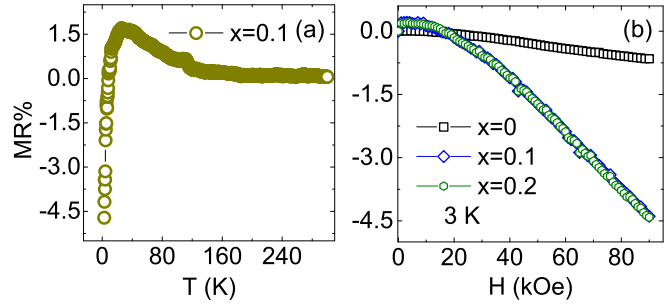

FIG. 9. (a) Temperature-dependent magnetoresistance for $x = 0.1$ compound. (b) Magnetic-field-dependent magnetoresistance at 3 K for $Eu_2(Ir_{1-x}Cu_x)_2O_7$, where $x = 0$, 0.1, and 0.2.

fitted C/T vs T^2 data with the formula

$$C = \gamma T + \beta T^3 \tag{4}$$

in the temperature region 2.1–6 K for all the compounds, as shown in Fig. 10(d). We obtain the γ value for the parent compound to be 32 mJ mol^{-1} K^{-2} which is consistent with the value reported by Ishikawa *et al.* [21]. From the inset of Fig. 10(d) we observe that γ abruptly decreases with Cu doping.

IV. DISCUSSION

In the parent $Eu_2Ir_2O_7$ compound, the transport property is driven by the 5*d* transition metal Ir. The transition metal is subjected to a trigonal distortion of the octahedral field. The ionic radii [29] of Cu^{2+}, Ir^{4+}, and Ir^{5+} are 0.87, 0.765, and

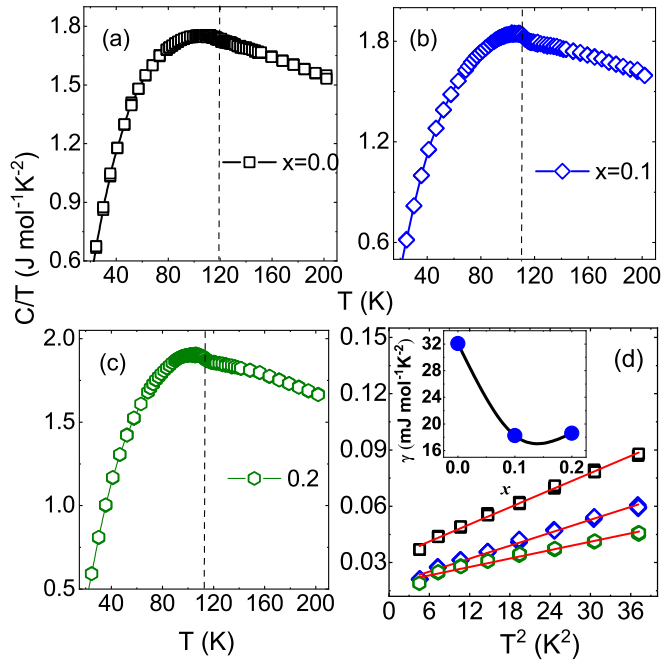

FIG. 10. (a)–(c) Plot of temperature-dependent specific heat (C/T) in the temperature range 20–200 K for the samples $Eu_2(Ir_{1-x}Cu_x)_2O_7$. (d) Representation of C/T vs T^2 plot for all the samples at low temperature. Solid red lines are fitted line. Inset: variation of the electronic contribution (γ) with Cu concentration.

0.71 Å, respectively, with coordination number six. As the ionic radius of Cu^{2+} is greater than Ir^{4+} each Cu at Ir site tends to increase the volume of the unit cell. On the other hand, each Cu will convert two nearby Ir^{4+} sites into Ir^{5+}, thereby contracting the unit cell. The overall effect is a reduction of lattice spacing with increasing Cu concentrations. When each Cu gives rise to two Ir^{5+} ions, this is like hole doping in a pyrochlore spin-$\frac{1}{2}$ antiferromagnet. This could lead to the reduction in T_{MI}, which was observed in the systems where Sr replaces Eu [19]. However, we did not see any significant change in T_{MI}, while Cu concentration increases from 10% to 20%. We believe that the energy level available at Cu site for an incoming electron is higher than the energy level of the electron at the Ir site. Hence, Cu^{2+} sites are not available for transport of d electrons on the Ir sublattice. These sites are effectively blocked for transport (though they retain their spin) and resistivity increases with Cu doping. The situation can be regarded as a percolation problem where sites are being removed randomly. T_{MI} is insensitive to Cu doping for concentration of more than 10% since it is beyond the $3d$ percolation limit.

At low-temperature region (below 50 K), the resistivity data follow power-law-like variation. Below T_{MI} the rise in Seebeck coefficient indicates the increase of insulating nature of the samples with Cu doping. A significant negative Hall voltage appearing at low temperature can be associated to a spin fluctuation influenced by the magnetic field. In this temperature region, the dominant charge carrier for all the compounds is electronlike, where carrier concentration decreases with Cu doping.

Both Ir and Cu have pseudo-spin-$\frac{1}{2}$ single-ion anisotropy but their orbitals are different. The ground-state spin arrangement of Ir is all-in–all-out (AIAO). There is an unavoidable nonstoichiometry in the parent compound [21,22], and it creates a nonmagnetic Ir^{5+} state, which deviates the spin structure from AIAO. Each of the tetrahedra picking a moment in an applied field forms field-induced ferrodroplets, which pinned within the background AIAO AFM spin. This further gives rise to exchange-bias-like behavior and increases with Cu doping due to an increase of the Ir^{5+} state. These ferrodroplets are randomly frozen in the AIAO AFM background matrix giving rise to the bifurcation in ZFC-FC magnetization depending on the amount and size of the droplets and they increase with Cu concentration.

For the parent compound MR is negative at low temperature with small magnitude, which varies quadratically at low field and linearly at high field. We proposed that such type of MR behavior is due to the chiral spin liquid [30–32]. Increase in Cu concentration reduces the AIAO AFM region which in turn reduces the region of spin-liquid phase as indicated in the specific-heat data. The doping of Cu increases the field-induced ferrocorrelated region and consequently the MR increases due to reduction of spin-flip scattering from the ferrodroplet region.

Now we would like to mention another important observation: the existence of linear specific heat for all the samples at low temperature. Generally, the linear specific heat at the insulating state arises from the weak localization due to finite density of state at the Fermi level. But, in our samples, resistivity data rule out the weak localization nature of the resistivity at the insulating state. On the other hand, the antiferromagnetic frustrated lattice often gives rise to a spin-liquid ground state, which supports fractional excitation, called spinon [33]. Spin liquid is a kind of spin superfluid (pairing between spinon with opposite spin), where spin excitations occur with or without a gap [34]. Theoretical study of an antiferromagnetic kagome lattice indicates that a linear specific heat at the insulating state can be possible if the spinons have finite-area Fermi surface [35]. Since Cu doping creates regions (droplets) of deviated AIAO structure and, thus, with increase in Cu doping the prerequisite condition for spin-liquid formation region decreases, which is observed in the specific-heat data. We also notice the onset of a negative Hall voltage in the temperature region where the spin-liquid state exists. This may be due to the spin fluctuation in the spin-liquid state, and needs to be addressed furthermore by theory.

V. CONCLUSION

From our analysis of magnetic, electrical, and thermal behavior of Cu-doped pyrochlore iridate $Eu_2(Ir_{1-x}Cu_x)_2O_7$, we conclude that each Cu creates two Ir^{5+} which deviates each corner-shared tetrahedron from its AIAO spin structure and picks up a magnetic moment. It does not support the spin-liquid state in the vicinity of Cu within a background of antiferromagnetically coupled AIAO spin structure. Observation of linear specific heat at low temperature indicates quantum spin fluctuation of spinons. With increasing Cu concentration, the coefficient of the linear specific heat decreases, indicating reduction of spinon density which is attributed to the reduction of the AIAO AFM region. Increase in resistivity below T_{MI} is due to the onset of AFM phase transition, and power-law-dependent increase in resistivity with lowering temperature indicates that it is neither an activated nor Mott variable range hopping as expected in a three-dimensional disordered system. At low temperatures, increase of resistance and sudden development of negative Hall voltage can be associated with the onset of spin-liquid formation. The doping of Cu increases the field-induced ferrocorrelated region and, as a result, the MR increases due to reduction of spin-flip scattering. The bifurcation observed in the ZFC-FC magnetization which increases with Cu doping is due to formation of randomly oriented blocked supermoments embedded in the AIAO AFM phase. Increase in exchange bias with Cu doping is due to the increase in the amount or size of pinning of the ferrospin within the AFM AIAO matrix of the system.

ACKNOWLEDGMENTS

S.M. would like to thank Prof. M. Mukherjee, Prof. S. Hazra, G. Sarkar, SPMS Division, SINP, for XPS measurement and Dr. M. K. Mukhopadhyay and Dr. R. Dev Das, SPMS Division, SINP, for XRD measurement. S.M. acknowledges UGC-DAE CSR, Kolkata, for Hall measurement and ECMP Division, SINP, for magnetic measurement. Authors acknowledge CIF, IISER Bhopal, for PPMS and SQUID-VSM facilities. This work is partially supported by SERB, DST, GOI under TARE project (Grant No. TAR/2018/000546).

[1] W. Witczek-Krempa, G. Chen, Y. B. Kim, and L. Balents, Annu. Rev. Condens. Matter. Phys. **5**, 57 (2014).

[2] Y. Yamaji, Y. Nomura, M. Kurita, R. Arita, and M. Imada, Phys. Rev. Lett. **113**, 107201 (2014).

[3] D. E. MacLaughlin, O. O. Bernal, L. Shu, J. Ishikawa, Y. Matsumoto, J.-J. Wen, M. Mourigal, C. Stock, G. Ehlers, C. L. Broholm, Y. Machida, K. Kimura, S. Nakatsuji, Y. Shimura, and T. Sakakibara, Phys. Rev. B **92**, 054432 s (2015).

[4] X. Wan, A. M. Turner, A. Vishwanath, and S. Y. Savrasov, Phys. Rev. B **83**, 205101 (2011).

[5] B. J. Kim, H. Jin, S. J. Moon, J.-Y. Kim, B.-G. Park, C. S. Leem, J. Yu, T. W. Noh, C. Kim, S.-J. Oh, J.-H. Park, V. Durairaj, G. Cao, and E. Rotenberg, Phys. Rev. Lett. **101**, 076402 (2008).

[6] Z. Tian, Y. Kohama, T. Tomita, H. Ishizuka, T. H. Hsieh, J. J. Ishikawa, K. Kindo, L. Balents, and S. Nakatsuji, Nat. Phys. **12**, 134 (2006).

[7] K. Matsuhira, M. Wakeshima, Y. Hinatsu, and S. Takagi, J. Phys. Soc. Jpn. **80**, 094701 (2011).

[8] D. Yanagishima and Y. Maeno, J. Phys. Soc. Jpn. **70**, 2880 (2001)

[9] D. Pesin and L. Balents, Nat. Phys. **6**, 376 (2010).

[10] H. Zhang, K. Haule, and D. Vanderbilt, Phys. Rev. Lett. **118**, 026404 (2017).

[11] B.-J. Yang and Y. B. Kim, Phys. Rev. B **82**, 085111 (2010).

[12] S. Nakatsuji, Y. Machida, Y. Maeno, T. Tayama, T. Sakakibara, J. van Duijn, L. Balicas, J. N. Millican, R. T. Macaluso, and J. Y. Chan, Phys. Rev. Lett. **96**, 087204 (2006).

[13] G. Chen and M. Hermele, Phys. Rev. B **86**, 235129 (2012).

[14] F. F. Tafti, J. J. Ishikawa, A. McCollam, S. Nakatsuji and S. R. Julian, Phys. Rev. B **85**, 205104 (2012).

[15] P. Hosur, S. A. Parameswaran, and A. Vishwanath, Phys. Rev. Lett. **108**, 046602 (2012).

[16] P. Telang, K. Mishra, G. Prando, A. K. Sood, and S. Singh, Phys. Rev. B **99**, 201112(R) (2019).

[17] I. N. Bhatti, R. S. Dhaka, and A. K. Pramanik, Phys. Rev. B **96**, 144433 (2017).

[18] H. Kumar, R. S. Dhaka, and A. K. Pramanik, Phys. Rev. B **95**, 054415 (2017).

[19] A. Banerjee, J. Sannigrahi, S. Giri, and S. Majumdar, Phys. Rev. B **96**, 224426 (2017).

[20] P. W. Anderson, Mater. Res. Bull. **8**, 153 (1973).

[21] J. J. Ishikawa, E. C. T. OFarrell, and S. Nakatsuji, Phys. Rev. B **85**, 245109 (2012).

[22] W. K. Zhu, M. Wang, B. Seradjeh, Fengyuan Yang, and S. X. Zhang, Phys. Rev. B **90**, 054419 (2014).

[23] N. Mott, *Conduction in Non-Crystalline Materials* (Clarendon, Oxford, 1993).

[24] P. Telang, K. Mishra, A. K. Sood and S. Singh, Phys. Rev. B **97**, 235118 (2018).

[25] D. K. C. MacDonald, *Thermoeectricity: An Interoduction to the Principles* (Dover, New York, 2006).

[26] S. Zhao, J. M. Mackie, D. E. MacLaughlin, O. O. Bernal, J. J. Ishikawa, Y. Ohta, and S. Nakatsuji, Phys. Rev. B **83**, 180402(R) (2011).

[27] H. Sagayama, D. Uematsu. T. Arima, K. Sugimoto, J. J. Ishikawa, E. O'Farrell, and S. Nakatsuji, Phys. Rev. B **87**, 100403(R) (2013).

[28] W. C. Yang, W. K. Zhu, H. D. Zhou, L. Ling, E. S. Choi, M. Lee, Y. Losovyj, C.-K. Lu, and S. X. Zhang, Phys. Rev. B **96**, 094437 (2017).

[29] M. W. Barsoum, *Fundamentals of Ceramics* (IOP Publishing, Bristol, 2003).

[30] Y. Machida, S. Nakatsuji, S. Onoda, T. Tayama, and T. Sakakibara, Nature (London) **463**, 210 (2010).

[31] T. C. Fujita, Y. Kozuma, M. Uchida, A. Tsukazaki, T. Arima, and M. Kawasaki, Sci. Rep. **5**, 9711 (2015).

[32] S. Mondal, M. Modak, B. Maji, M. K. Ray, S. Mandal, S. K. Mandal, M. Sardar, and S. Banerjee, Phys. Rev. B **102**, 155139 (2020).

[33] L. Balents, Nature (London) **464**, 199 (2010).

[34] G. Baskaran, Z. Zou, and P. W. Anderson, Solid. State Commun. **63**, 973 (1987).

[35] Y. Ran, M. Hermele, P. A. Lee, and X. G. Wen, Phys. Rev. Lett. **98**, 117205 (2007).